Supplement of Atmos. Chem. Phys., 14, 11557–11569, 2014
http://www.atmos-chem-phys.net/14/11557/2014/
doi:10.5194/acp-14-11557-2014-supplement

Atmospheric Chemistry and Physics Open Access

Supplement of

Composition of 15–85 nm particles in marine air

M. J. Lawler et al.

Correspondence to: M. Lawler (mlawler@ucar.edu)

Supplemental Material for
Composition of 15-80 nm particles in marine air
Lawler et al., 2013

S1. Collected Aerosol Mass

As stated in the manuscript, the mass of particles collected for each TDCIMS analysis point was estimated using an inverse model which used data from a condensation particle counter (CPC) downstream from the TDCIMS and from a scanning mobility particle sizer (SMPS) sampling ambient air.

The CPC monitored particle number concentrations downstream from the TDCIMS electrostatic precipitator (or, briefly, the "wire"). When a collection voltage was applied to the wire, the number concentration dropped, and the decrease was attributed entirely to particles being deposited on the wire. The efficiency of particle collection was assessed by comparing "collection" and "background" (no wire voltage) particle counts for periods of relatively stable particle concentrations, for each of the TDCIMS RDMA settings used: 15 , 20, and 30 nm mobility diameter for singly charged particles. Efficiencies were 0.22, 0.22, and 0.14, respectively. Higher efficiencies are achievable, but at a cost of exposing more of the wire to sample air and thereby risking more contamination by gas phase species. Knowing the collection efficiencies for each RDMA setting, the CPC-measured particle number for all collection periods, and the collection time allows the calculation of the number of collected particles. However, the width of the RDMA transfer function and the occurrence of multiple charging in the unipolar chargers (UPCs) make it impossible to accurately estimate the actual particle volume collected without knowing something about the size distribution of sampled particles and the efficiencies with which differently-sized particles are sampled and ionized.

Tests were performed in the laboratory at NCAR to establish the RDMA passing efficiencies as functions of particle electrical mobility for the three different RDMA settings used in the present study. The extent of multiple charging was also examined. These investigations were performed by delivering a steady concentration of particles to a UPC and RDMA operated as they were at Mace Head and monitoring the output from the RDMA with an SMPS system comprised of a DMA (TSI 3081) and CPC (TSI 7610). A ^{210}Po bipolar charger was alternately included and removed between the RDMA and long DMA to place an equilibrium bipolar distribution of charge on the particles to reveal larger particles which had been multiply charged when they passed the RDMA. These experiments showed clear evidence for particle charges of 1-3 elementary charges and a relatively wide RMDA mobility window for all three standard RDMA settings (e.g. >20% passing efficiency for a ~ 9 nm window in the case of "20 nm" particles). The mass collected on the wire is therefore highly dependent on the ambient particle size distribution and the sampling efficiencies of particles of different sizes.

In order to estimate the collected particle mass, a best-fit size-resolved sampling efficiency was calculated for each RDMA setting and applied to each TDCIMS collection. This was done by minimizing a cost function defined as the sum of squared differences between mean CPC concentrations during collections and modeled mean particle concentrations. The model assigned a TDCIMS sampling efficiency for each size bin in the site SMPS. This size-resolved sampling efficiency was implemented as a sum of three Gaussian functions (of size) for which the amplitude, center, and width were all independently variable (a total of nine independent parameters). Each Gaussian was intended to represent the distribution about a central particle size for each of the three charge states expected to be present after UPC charging and RDMA selection: 1e, 2e, and 3e where e is the charge of one electron. Acceptable ranges for the parameters were specified based on laboratory-observed passing efficiency windows for the RDMAs and calculated electrical mobilities for singly, doubly, and triply charged particles (Table S1). The model was optimized using a time series of CPC and SMPS data of at least 22 half-hour-averaged points for each RDMA set voltage. The specific algorithm used was Optimize with simulated annealing in Igor Pro 6.22. The model was iterated at least 10,000 times for each of the three RDMA settings. The optimization was performed many times, and in the case of "20 nm" and "30 nm" RDMA settings, for different time periods. The results were qualitatively similar but not identical for the different attempts, and the model always accounted for over 90% of the variance in the CPC data. The results of the optimizations which were used to generate Figure 1c. in the manuscript are presented in Figure S1.

For each RDMA setting, there is a significant peak near the nominal set point (the singly-charged particles) and then a secondary peak which can be quite broad and physically represents the doubly and triply charged sizes. The passing efficiencies of the "15" and "20 nm" particles are about half that of the 30 nm particles, perhaps due to greater depositional losses in the sample line (Figure S1). The separation between the singly charged peak and the broad 2- and 3-charge peak is large in the 30 nm case due to a proportionally greater mobility impact of additional charge for larger particles. Larger particles are more likely to be multiply charged, so it is unsurprising that selecting for smaller sizes results in the sampling for particles closer to the nominal set point.

It is important to note that the size-resolved efficiencies have many effects folded into them: inlet sampling and transport efficiency, (multiple) charging efficiency, and RDMA passing efficiency. We make no attempt here to explicitly tease out the various effects individually. These results are therefore an empirical fit to the data, despite being founded on processes which we know occur. The fact that similar results are obtained for multiple runs given a realistic and fairly wide range of acceptable parameter values indicates that the solutions are fairly robust. The high explanatory power of the model shows that there is a real and consistent link between the ambient SMPS data and TDCIMS CPC data (Figure S2). This should not be surprising, but it suggests that the TDCIMS sampling efficiencies were relatively

constant over time and that the SMPS and TDCIMS were sampling the same air most of the time.

Size (nm)	D_0 (nm)	a_0	D_1 (nm)	a_1	D_2 (nm)	a_2	w_n (n=1,2,3)
15	14-19	0.2-1	18-24	0.001-0.8	22-28	0.001-0.8	0.001-0.01
20	21-25	0.2-1	27-35	0.001-0.5	33-42	0.001-0.5	0.001-0.01
30	25-35	0.2-1	39-48	0.001-0.5	49-59	0.001-0.5	0.001-0.01

Table S1. Acceptable ranges for model parameters for the equation $f(\boldsymbol{X}) = \sum_{n=0}^{2} a_n e^{-\frac{(\boldsymbol{X}-D_n)}{2w_n^2}}$ where f is the efficiency as a function of size $\boldsymbol{X}$. Parameters given for each nominal RDMA setting: 15, 20, or 30 nm mobility diameter for a singly charged particle. *D*'s are the central size, and *a*'s are the amplitude (maximum collection efficiencies) for each of the three Gaussians fit. The actual central sizes were biased slightly high from the nominal RDMA set points, and this is reflected in the *D* values chosen.

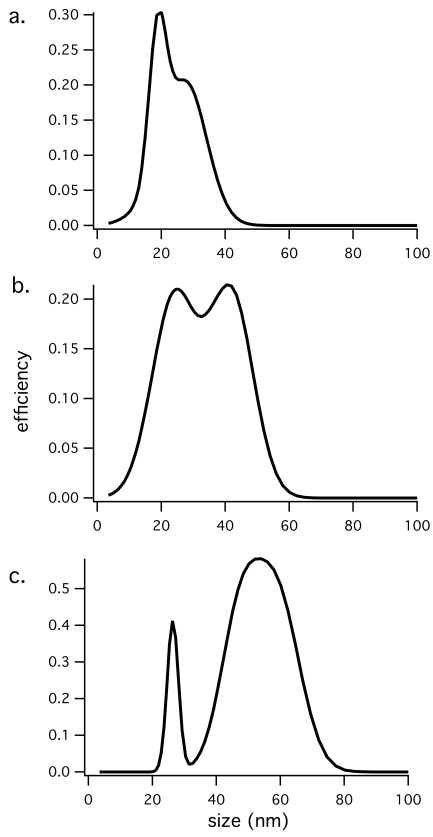

Figure S1a. Results of the inverse model for passing efficiency of particles reaching the TDCIMS CPC. These efficiencies represent the net effects of sampling, unipolar

charging, and size selection by RDMA for each of the three nominal RMDA settings used at Mace Head: **a**. 15 nm, **b**. 20 nm., **c**. 30 nm.

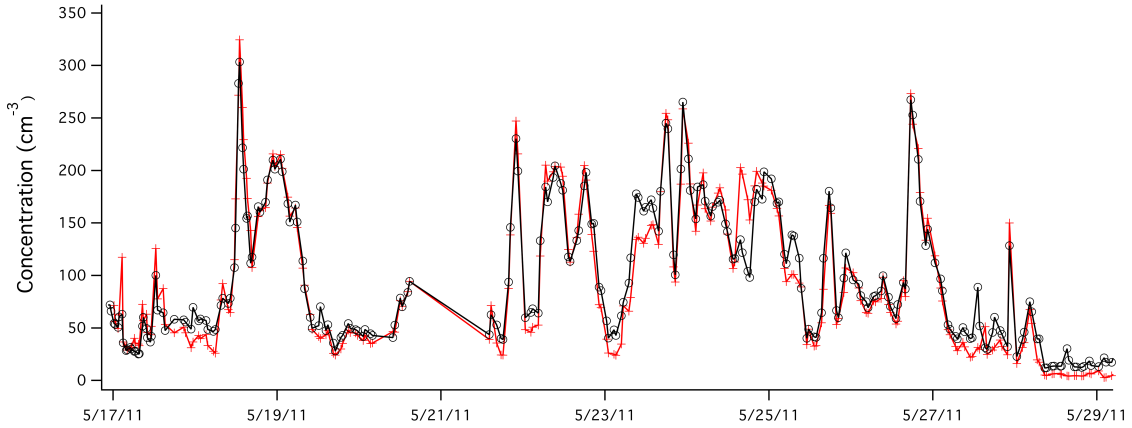

Figure S1b. Comparison of measured particle concentrations at the TDCIMS CPC (black circles and lines) with model-derived particle concentrations after optimizations (red crosses and lines).

S2. TDCIMS Desorption Thermogram

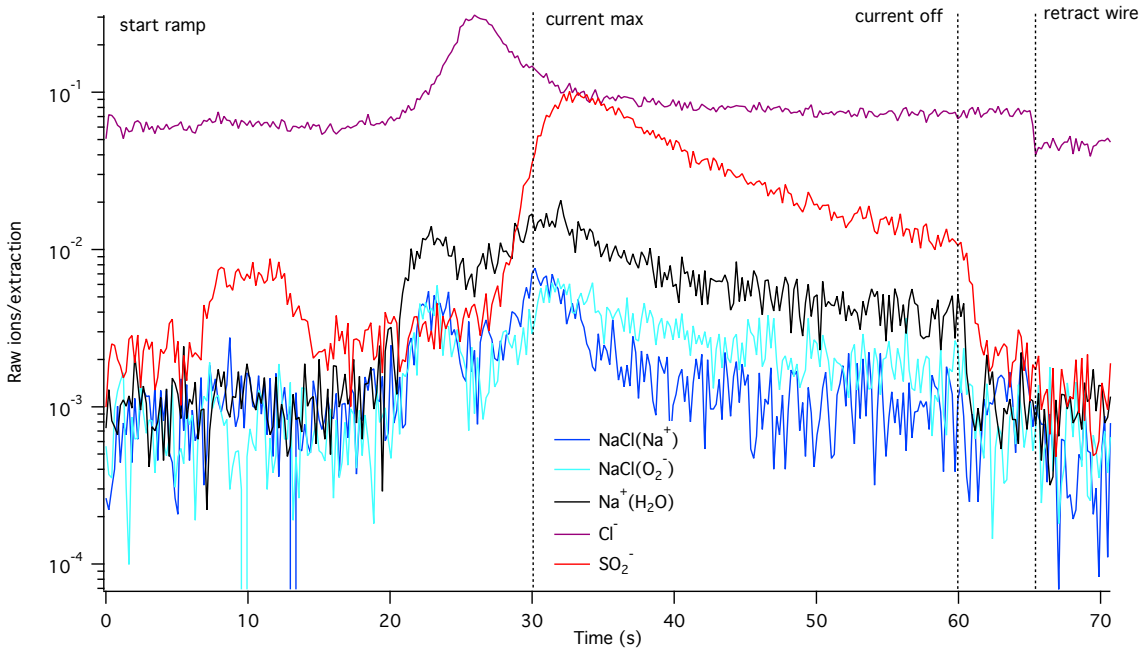

Figure S2. A single ambient sample desorption thermogram from May 25, 2011 for unit mass resolution peaks. The main species associated with each nominal mass are indicated. Times when current was applied to the wire are indicated.